High resolution pulsed field ionization photoelectron spectroscopy using multibunch synchrotron radiation: Time-of-flight selection scheme

G. K. Jarvis
Chemical Science Division, Lawrence Berkeley National Laboratory, Berkeley, California 94720

Y. Song and C. Y. Ng[a)]
Ames Laboratory, United States Department of Energy and Department of Chemistry, Iowa State University, Ames, Iowa 50011

(Received 4 January 1999; accepted for publication 24 February 1999)

We have developed an efficient electron time-of-flight (TOF) selection scheme for high resolution pulsed field ionization (PFI) photoelectron (PFI-PE) measurements using monochromatized multibunch undulator synchrotron radiation at the Advanced Light Source. By employing a simple electron TOF spectrometer, we show that PFI-PEs produced by the PFI in the dark gap of a synchrotron ring period can be cleanly separated from prompt background photoelectrons. A near complete suppression of prompt electrons was achieved in PFI-PE measurements by gating the PFI-PE TOF peak, as indicated by monitoring background electron counts at the $Ar(11s')$ autoionizing Rydberg peak, which is adjacent to the $Ar^+(^2P_{3/2})$ PFI-PE band. The rotational-resolved PFI-PE band for H_2^+ $(X\,^2\Sigma_g^+, v^+=0)$ measured using this electron TOF selection scheme is nearly free from residues of nearby autoionizing features, which were observed in the previous measurement by employing an electron spectrometer equipped with a hemispherical energy analyzer. This comparison indicates that the TOF PFI-PE scheme is significantly more effective in suppressing the hot-electron background. In addition to attaining a high PFI-PE transmission, a major advantage of the electron TOF scheme is that it allows the use of a smaller pulsed electric field and thus results in a higher instrumental PFI-PE resolution. We have demonstrated instrumental resolutions of 1.0 cm^{-1} full width at half maximum (FWHM) and 1.9 cm^{-1} FWHM in the PFI-PE bands for $Xe^+(^2P_{3/2})$ and $Ar^+(^2P_{3/2})$ at 12.123 and 15.760 eV, respectively. These resolutions are more than a factor 2 better than those achieved in previous synchrotron based PFI-PE studies. © *1999 American Institute of Physics.*
[S0034-6748(99)02006-7]

I. INTRODUCTION

Pulsed field ionization (PFI) photoelectron (PFI-PE) detection schemes are superior as spectroscopic techniques in terms of achievable resolutions compared to conventional threshold photoelectron (TPE) measurements.[1–3] In the discussion below, we refer to PFI-PEs and TPEs as electrons formed at energies slightly below and above, respectively, the true ionization energy (IE). The most common TPE detection schemes incorporate a steradiancy-type analyzer,[4–7] which is essentially a tube-like structure that defines a finite solid angle for the acceptance of electrons. Since TPEs are formed with near zero kinetic energies, their collection can be achieved using a small dc electric field, whereas hot or prompt electrons ejected isotropically with finite kinetic energies are strongly discriminated by the specific acceptance solid angle of the steradiancy analyzer. Since hot electrons moving directly towards the detector are not discriminated against, the transmission function of such analyzers results in a high-energy tail, that consequently limits the attainable resolution in TPE measurements. When an ionization threshold is close to strong autoionizing Rydberg states, undesirable residues of these nearby autoionization states are often observed in addition to the TPE peaks. The hot-electron tail of the transmission function can be reduced by combining the electron time-of-flight (TOF) technique[8,9] or by adding a differential energy analyzer, such as a hemispherical energy analyzer, in tandem to the steradiancy analyzer.[10] The employment of a differential energy analyzer has the disadvantage of lowering the electron transmission. Incorporating the electron TOF scheme in synchrotron based TPE measurements, Morioka and co-workers have demonstrated a resolution of 1 meV full width at half maximum (FWHM).[11] However, this TOP-TPE method generally requires a single- or two-bunch synchrotron operation,[8,9,11] in which adjacent synchrotron light pulses are separated by ≈300 ns. Since the reduction in vacuum ultraviolet (VUV) intensities in a single- or a two-bunch mode is more than a factor of 10 compared to that in a multibunch operation, the application of the TOF-TPE scheme has been limited in synchrotron based TPE measurements.

The laser based PFI-PE techniques[1–3] have been shown to overcome the hot-tail problem associated with the TPE transmission function. In the UV/VUV laser PFI-PE schemes, the PFI electric field, which ionizes high-*n* Rydberg species formed by photoexcitation, is delayed by a few

[a)]Author to whom correspondence should be addressed; electronic mail: cyng@ameslab.gov

μs relative to the light pulse, thus allowing the prompt background electrons to escape from the detection zone and be eliminated from the final spectra. There is general agreement that the extended lifetimes for high-n Rydberg states observed in PFI-PE experiments are due to l and m_l mixings induced by stray electric fields and/or by coexisting background ions formed during laser–molecule interactions.[13,14] The PFI-PE resolution depends on both the laser optical bandpass and the strength (F) of the electric field pulse. Since the width[15] of PFI-PEs is proportional to $F^{1/2}$, the key to achieve a high PFI-PE resolution with a fixed optical bandpass is to apply a small F for the PFI. It has been shown previously that PFI-PE resolutions close to the laser optical bandpass are attainable.[1]

Recently, a novel synchrotron based PFI-PE experimental scheme has been developed by our group at the chemical dynamics beamline of the Advanced Light Source (ALS).[10,16–18] These experiments make use of the dark gap of 16–112 ns in the ALS synchrotron ring period to apply the ionizing electric field pulse. Using an electron spectrometer consisting of a steradiancy analyzer and a hemispherical energy analyzer arranged in tandem, we have shown that PFI-PEs can be detected with little contamination from prompt electron background for a delay of only $\approx$8 ns with respect to the beginning of the dark gap.[10,16,17] Limited by the nature of the previous synchrotron based PFI-PE scheme and also by a typically poorer optical resolution than that of UV/VUV lasers, the best PFI-PE resolution achieved was 3.2 cm^{-1} (FWHM) as illustrated in the observed PFI-PE band of $Kr^+(^2P_{3/2})$.[17] In previous PFI-PE experiments from the ALS, the minimization of prompt electron contaminations from nearby autoionizing states relies partly on the chromatic aberration of the electrostatic lens system.[10] In order to achieve a high PFI-PE transmission through the electron spectrometer, it is necessary to apply a sufficiently high pulsed electric field, which essentially sets the limit for the attainable PFI-PE resolution.[10] Even with extreme care in optimizing the PFI-PE electron spectrometer, a small high-energy transmission tail is still discernible in most previous synchrotron based PFI-PE measurements.[10,16–18] The discrimination of hot-electron background can be monitored by the electron counts at an energy corresponding to the Ar($11s'$) Rydberg state, which lies $\approx$4.3 meV higher in energy than the $Ar^+(^2P_{3/2})$ PFI-PE band.[10,16,17] The background electron intensity at Ar($11s'$) is usually found to be $\sim$1% of that at the $Ar^+(^2P_{3/2})$ PFI-PE peak. Although small, this incomplete suppression may still hamper identification of weak PE bands, especially in the presence of strong autoionizing structure.[18]

In this article, we describe a highly efficient synchrotron based PFI-PE detection method, which takes advantage of the TOF difference of prompt electrons and PFI-PEs. By employing a simple electron TOF spectrometer, we show that almost complete separation of PFI-PEs and prompt background electrons can be achieved. The gating of the PFI-PEs thus leads to a near complete suppression of prompt electrons. In the previous PFI-PE study of H_2^+ ($X\,^2\Sigma_g^+ v^+ = 0$, 2, 9, and 11),[18] the PFI-PE spectra are found to be contaminated by residue peaks arising from many strong autoionizing Rydberg resonances. Consequently, the observed relative PFI-PE peak intensities may not reflect the actual PFI-PE cross sections. We show here that the PFI-PE band for $H_2^+(X\,^2\Sigma_g^+ v^+ = 0)$ obtained using this new TOF PFI-PE scheme is essentially free from residues of strong autoionizing structures observed in the previous measurement.[18] Hence, the H_2^+ PFI-PE band recorded in this experiment should provide more reliable PFI-PE cross sections.

Furthermore, since the electron transmission of the TOF PFI-PE selection scheme is not strongly affected by the pulsed electric field for the PFI, a lower Stark electric field pulse can be used. This leads to higher achievable PFI-PE resolutions. To illustrate this advantage, we show below the PFI-PE bands for $Xe^+(^2P_{3/2})$ and $Ar^+(^2P_{3/2})$ recorded using the TOF PFI-PE method, achieving resolutions unmatched in previous synchrotron based PFI-PE experiments.[10,16–18]

II. EXPERIMENTAL CONSIDERATIONS

The experiments were carried out at the Chemical Dynamics Beamline[19–21] of the ALS associated with the Lawrence Berkeley National Laboratory. The beamline consists of a 10-cm-period undulator, a gas harmonic filter,[21] a 6.65-m-off-plane Eagle mounted monochromator and a photoelectron–photoion spectrometer, all of which have been described in detail previously.[10,16–21] In this experiment, Ar was used as the filter gas and thus high undulator harmonics at energies above the IE of Ar (15.760 eV) were essentially eliminated. The filtered undulator VUV light beam, which consists of predominantly the first undulator harmonic, was directed into the monochromator, where the VUV photon beam was dispersed by either a 2400 lines/mm grating (dispersion=0.64 Å/mm) or a 480 lines/mm (dispersion=0.32 Å/mm). The resulting monochromatic VUV beam was then focused into the photoionization/photoexcitation (PI/PEX) region of the photoelectron–photoion apparatus. In this experiment, monochromator entrance/exit slits used were either 10/10 or 30/30 μm. The photon energy calibration was achieved using the known IEs or photoionization transitions of Ar, Xe, and H_2.[17–19] All gas samples were introduced as an effusive beam through a metal orifice with a diameter of 0.5 mm at room temperature and a distance of 0.5 cm from the PI/PEX region.

The electron TOF spectrometer used in this study has been modified from the one used in our previous experiments.[10,16–19] The main difference was that the hemispherical analyzer has been removed and only a steradiancy analyzer was used as an electron TOF spectrometer. A schematic diagram showing the present lens arrangement for the electron and ion TOF detection can be seen in Fig. 1. The distance between lenses I1 and E1 was 1.0 cm. The midpoint between lenses I1 and E1 defined the PI/PEX region. The apertures in lenses E1 and E4 used here were 10 and 2 mm in diameter, respectively. Microspherical plates (MSP) were used as the electron and ion detectors.

The PFI schemes employed here and previously[13–19] make use of the dark gap—a short time lapse in every ring period, where no synchrotron light is emitted from the source. Typical operating conditions for the ALS have been

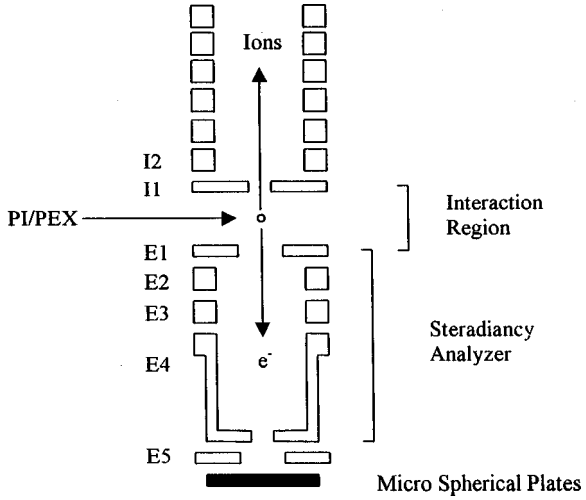

FIG. 1. Schematic diagram showing the electrostatic lens arrangement, the ion and electron TOF spectrometer. The electron and ion detectors are microspherical plates (MSP). The ion drift tube and the ion MSP detector are not shown in the figure.

changed slightly from our previous publications[16–18,20–26] to accommodate the various different timing experiments that take place at our and other beamlines. Currently, the entire orbit contains 272 bunches each of 50 ps duration and separated by 2 ns. There is a 112-ns-dark gap at the end of each ring period for removing ions formed in the orbit. Occasionally, a high current spike (typically 10 mA) is injected into the dark gap at bunch 312 relative to the first bunch after the dark gap. Even with this spike present, a true dark gap of 80 ns after the last of the multibunches is present, which is sufficient for performing our experiment, although electron discrimination is slightly poorer. All experiments presented here were carried out during the normal multibunch operation of the ALS with no high-current spike, i.e., with a dark gap of 112 ns. However, we note that the TOF PFI-PE selection scheme described below can be implemented with a dark gap down to 80 ns.

Here, we use Ar as the gas sample to illustrate the TOF-PFI-PE selection method. In this scheme, a dc voltage of -0.14 V was applied to lens I1 for the purpose of hot electron extraction. Prior to the application of the electric field pulse, lens E1 was set at the ground potential. This has the effect of pushing hot electrons arising from autoionization and direct ionization towards the electron detector as soon as they were formed. Typical voltages applied to lenses I2, E2, E3, E4, and E5 were -20, 0.5, 3.0, 2.0, and 500 V, respectively. The front grid of the MSP was set at 500 V. The electron flight distance is 6.8 cm, which was determined by the distance between the PI/PEX region and E5. This flight distance, along with the voltage settings for the lenses, determines the TOF of prompt electrons. The TOF for PFI-PEs also depends on the height and width of the electric field pulse applied for the Stark field ionization.

Figure 2(a) shows the emitting pattern of the ALS light pulses in the multibunch operation. The two shaded areas represent stacks of uniformly spaced synchrotron microlight bunches (width of individual bunches $=50$ ps, separation between adjacent bunches $=2$ ns). For clarity, the 112 ns

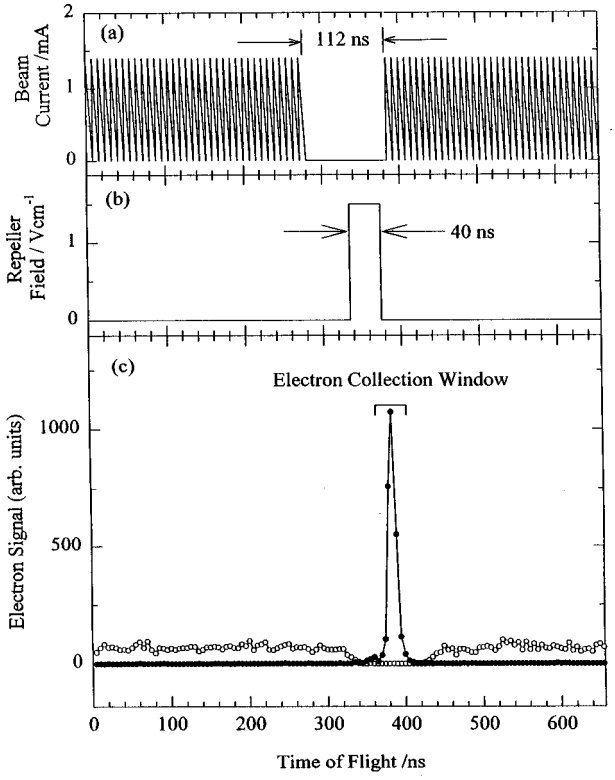

FIG. 2. The timing structures for (a) the pattern of VUV light bunches emitted in the ALS multibunch mode; (b) the electric field pulses applied to lens E1 (see Fig. 1); and (c) the electron TOF spectra of PFI-PEs (●) as observed at the $Ar^+(^2P_{3/2})$ PFI-PE peak and hot or prompt electrons (○) as observed at the $Ar(11s')$ autoionizing state.

dark gap is shown centered in the 656-ns-ring period in Fig. 2(a). Following a delay of some 20–60 ns with respect to the beginning of the dark gap, an electric field pulse in the range of 0.3–1.5 V/cm was applied to lens E1 [see Fig. 2(b)]. The frequency of the electric field pulse for the PFI was 1.53 MHz, consistent with the ring period.

When the photon energy was set to coincide with the $Ar^+(^2P_{3/2})$ PFI-PE peak at 15.7596 eV, the observed TOF spectrum (solid circles) for PFI-PEs was found to exhibit a single peak with a full width of $\approx$40 ns as shown in Fig. 2(c). We note that the time zero of the TOF spectra shown in Fig. 2(c) corresponds to the triggering bunch-marking pulse provided by the ALS, the position of which is arbitrary. Partly due to the small VUV spot size (0.2×0.3 mm^2) at the PI/PEX region,[19] the observed TOF peak for PFI-PEs was expected to be narrow. We note that the observed full width of 40 ns is equal to the width of the electric field pulse for the PFI. This observation indicates that the PFI-PEs formed within 40 ns during the application of the Stark pulses were highly monoenergetic with little dispersion as they traveled from the PI/PEX region to the electron MSP detector. No prompt electrons can be observed at 15.7596 eV because this energy is below the IE of Ar. It can be seen from the comparison with the positions of the Stark pulse [Fig. 2(b)] and the TOF peak for PFI-PEs that the TOF for PFI-PEs from the PI/PEX region to the electron MSP detector is $\approx$50 ns. As the photon energy was slightly increased above the IE for the formation of $Ar^+(^2P_{3/2})$, the single TOF peak for PFI-PEs

disappears and an electron TOF spectrum for prompt electrons resembling the synchrotron orbit pattern was observed as these electrons are extracted continuously by the small dc field. The electron TOF spectrum (open circles) observed using a 1.5 V/cm Stark pulse with the photon energy set at 15.7655 eV corresponding to the position of the Ar($11s'$) autoionizing Rydberg state is also shown in Fig. 2(c). In this spectrum, a small electron signal due to prompt electrons was observed uniformly in time except in a window of ≈110 ns corresponding to the width of the dark gap, where essentially no electrons were formed.

The location of the TOF peak for PFI-PEs in the TOF spectrum depends on the height of the Stark pulse and the delay with respect to the beginning of the dark gap. These parameters were adjusted so that the TOF peak for the PFI-PEs fell in the middle of the 110-ns-TOF window where no hot electrons were observed and thus achieved a clear separation of prompt electrons from PFI-PEs. As a result, PFI-PEs can be easily detected free from background prompt electrons by setting a gate with a width corresponding to the width of the TOF peak for PFI-PEs as shown in Fig. 2(c).

The gating of the PFI-PE counts was done using a LeCroy Model 622 coincidence unit. The timing or bunch-marker pulse from the ALS was a NIM pulse that was ≈24 ns wide. This pulse was typically shaped down to 4 ns using a Stanford Research Systems (SRS) pulse generator. The PFI-PE signal arrived at the electron MSP was passed first through an amplifier and then a discriminator. The resulting PFI-PE signal pulse was further shaped using another SRS pulse generator to the range of 1–10 ns. In the present experiment, the width of the shaped PFI-PE signal pulse was typically set at 10 ns. The coincidence unit received the shaped bunch-marker pulse and the shaped PFI-PE signal pulse as inputs. We then changed the delay of the shaped PFI-PE signal pulse until it overlapped with the shaped bunch-marker pulse. The coincidence unit only gave out an output pulse when the two pulses overlap. The minimum overlap between the two pulses is 1 ns. For a typical pulse width of 4 ns for the shaped bunch-marker pulse and that of 10 ns for the shaped electron signal pulse, the TOF resolution or effective gate width was 16 ns. Higher TOF resolutions down to 1 ns can be obtained, though this proved unnecessary due to the adequate separation of electron TOFs. We have used a gate width varied in the range of 20–40 ns and found that the increase of the PFI-PE counts was small. The prompt electron suppression efficiency decreases rapidly when the gate width was increased to >40 ns, in accordance with the TOF spectra observed in Fig. 2(c). We note that the width of the PFI-PE TOF peak depends on the height and width of the Stark pulse.

We found that even with lenses I1 and E1 held at 0 V dc, field penetration from adjacent lenses I2 and E2 still allowed for extraction of the prompt electrons toward the electron detector with sufficient time separation for discrimination. The TOF spectrum for prompt electrons observed with the photon energy set at the Ar($11s'$) autoionizing Rydberg state using a nominal dc repeller field of 0 V/cm for the PI/PEX region was similar to that (open circles) shown in Fig. 2(c).

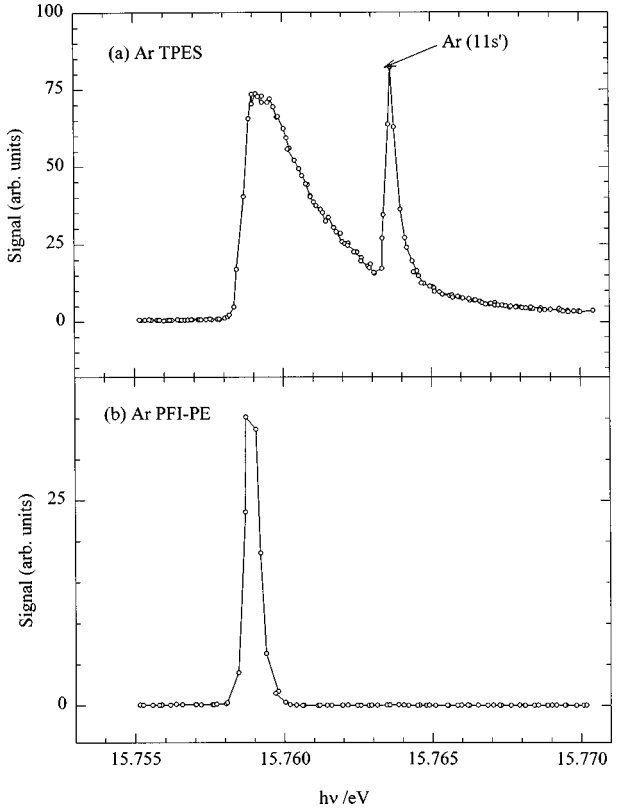

FIG. 3. (a) TPE spectrum for Ar in the range 15.755–15.770 eV observed by collecting all electrons arrived at the electron MSP detector. The electron TOF spectrometer was used as a steradiancy analyzer. (b) PFI-PE spectrum for Ar in the range 15.755–15.770 eV obtained using the TOF PFI-PE selection scheme. The 2400 lines/mm was used. The monochromator entrance/exit slits are set at 30/30 μm for both (a) and (b) corresponding to a nominal wavelength resolution of 0.0192 Å (FWHM).

III. RESULTS

In order to illustrate the superior performance of the TOF PFI-PE scheme as compared to the previous synchrotron based PFI-PE method.[16–18,22–26] in terms of the achievable resolution and prompt electron background suppression, we show below the PFI-PE spectra for $Ar^+(^2P_{3/2})$, $Xe^+(^2P_{3/2})$, and $H_2^+(v^+=0,N^+)$ obtained using the TOF PFI-PE method.

A. PFI-PE bands for $Ar^+(^2P_{3/2})$ and $Xe^+(^2P_{3/2})$

Figure 3(a) depicts the photoelectron spectrum for Ar in the region of 15.755–15.770 eV observed by collecting all electrons arriving at the electron MSP detector. In this case, the electron TOF spectrometer performed as a steradiancy analyzer for TPE detection. The 2400 lines/mm grating was used with monochromator entrance/exit slits set at 30/30 μm. As expected, the spectrum shown in Fig. 3(a) is essentially a TPE spectrum exhibiting the characteristic hot electron tail. The intensity of the autoionizing Ar($11s'$) Rydberg peak [marked in Fig. 3(a)] is stronger than that of the $Ar^+(^2P_{3/2})$ TPE peak. The PFI-PE band for $Ar^+(^2P_{3/2})$ depicted in Fig. 3(b) was recorded using a nominal dc field of 0 V/cm across lenses I1 and E1 and a 1.5 V/cm pulsed electric field of 40 ns duration for the PFI. As shown in Fig. 3(b), a near complete

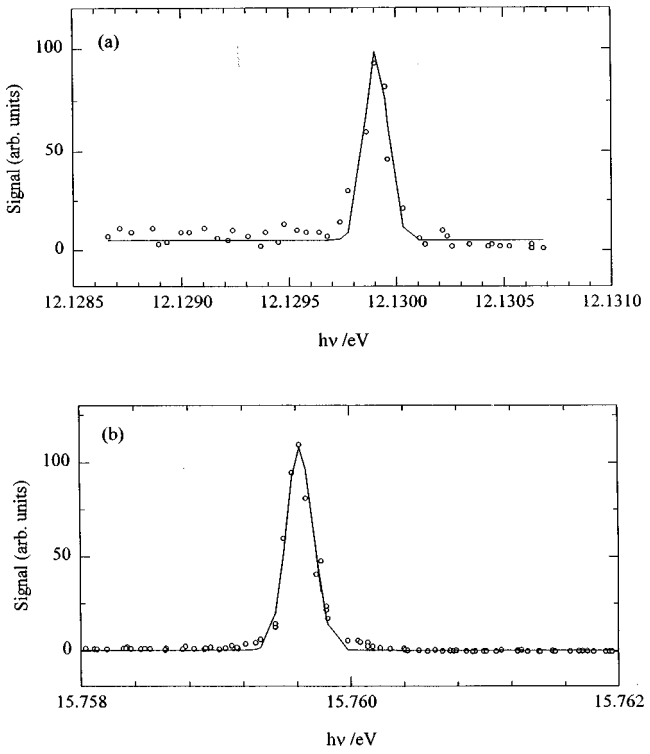

FIG. 4. (a) PFI-PE band for $Xe^+(^2P_{3/2})$ (open circles) obtained using a pulsed field of 0.3 V/cm. A Gaussian fit obtained using a least-squares fit is also shown (line), revealing a FWHM maximum of 1.0 ± 0.2 cm^{-1}. (b) Experimental PFI-PE band for $Ar^+(^2P_{3/2})$ (open circles) obtained using a pulsed field of 0.3 V/cm. A Gaussian fit obtained using a least-squares fit is also shown (line), revealing a FWHM of 1.9 ± 0.3 cm^{-1}. The 4800 lines/mm grating was used. The monochromator entrance/exit slits are set at 30/30 μm for both (a) and (b) corresponding to a nominal wavelength resolution of 0.0096 Å (FWHM).

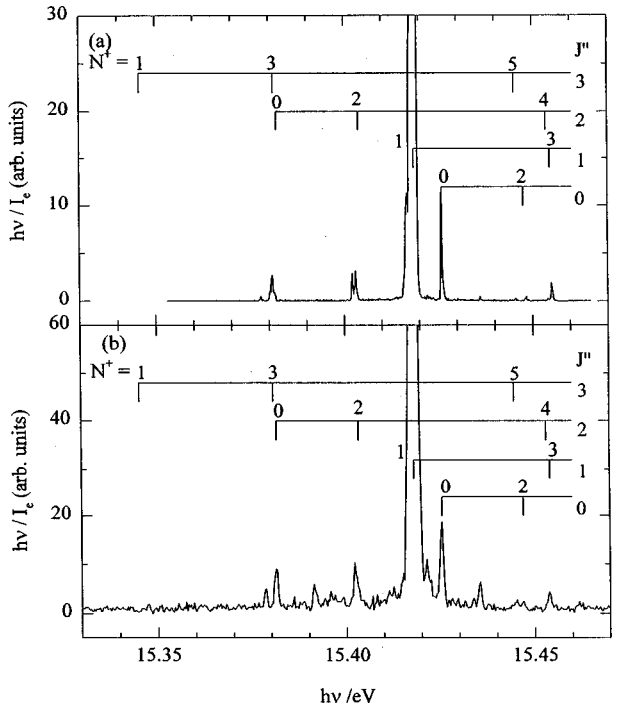

FIG. 5. PFI-PE spectrum for $H_2^+(X\,^2\Sigma_g^+, v^+=0)$ recorded (a) using electron TOF analysis with a 0 V/cm dc field, and a 1.5 V/cm pulsed field across the interaction region. The 4800 lines grating was used. The monochromator entrance/exit slits are set at 10/10 μm corresponding to a nominal resolution of 0.0064 Å (FWHM), (b) using a hemispherical and steradiancy analyzer in tandem and a 0.67 V cm^{-1} pulsed field at a nominal wavelength resolution of 0.048 Å (FWHM).

suppression of the Ar($11s'$) was achieved. The actual intensity at Ar($11s'$) was $<0.2\%$ of the $Ar^+(^2P_{3/2})$ intensity when the above TOF gating scheme was incorporated. This is approximately 10 times better than previous results obtained using a hemispherical analyzer for PFI-PE detection.[10]

As pointed out above, the previous PFI-PE detection scheme using a hemispherical energy analyzer requires a sufficiently high Stark pulse for attaining a high electron transmission. The relatively high Stark pulse required also limits the attainable PFI-PE resolution. The transmission of PFI-PEs in this TOF selection scheme does not have a strong dependence on the applied pulsed electric field. Figures 4(a) and 4(b) show the PFI-PE bands of $Xe^+(^2P_{3/2})$ and $Ar^+(^2P_{3/2})$ in the regions of 12.128–12.131 and 15.758–15.762 eV, respectively, measured using the TOF PFI-PE detection method. The pulsed field used in these measurements was $\approx$0.3 V/cm. The Gaussian fit to these PFI-PE spectra reveals a resolution of 1.0 cm^{-1} (FWHM) for the $Xe^+(^2P_{3/2})$ bands and 1.9 cm^{-1} (FWHM) for the $Ar^+(^2P_{3/2})$ band. These resolutions are more than a factor of two better than the best resolutions recorded for these PFI-PE bands in previous ALS experiments and are close to the best resolution (0.8 cm^{-1}, FWHM) reported using VUV laser PFI-PE techniques at $\approx$18 eV.[27] The resolutions of these spectra are limited by both the VUV optical resolution and the pulsed field used. We expect that the optical resolution can be improved by operating the monochromator in second or third order. Hence, the attainable resolution for this TOF PFI-PE method can be further improved.

B. PFI-PE band for $H_2^+(X\,^2\Sigma_g^+, v^+=0)$

The PFI-PE spectrum for $H_2^+(X\,^2\Sigma_g^+, v^+=0)$ in the energy range of 15.34–15.47 eV obtained using the TOF PFI-PE scheme with a 0 V/cm dc field at the PI/PEX region and 1.5 V/cm Stark pulsed field is depicted in Fig. 5(a). Using the 2400 lines/mm grating and monochromator entrance/exit slits sizes of 10/10 μm, the nominal wavelength resolution used was 0.0064 Å (FWHM). Figure 5(b) shows the $H_2^+(X\,^2\Sigma_g^+, v^+=0)$ spectrum in the same energy range recorded previously using a tandem steradiancy–hemispherical spectrometer at a nominal optical resolution of 0.048 Å [see Fig. 5(b)].[18] We note that the actual resolution is always lower than the nominal resolution. On the basis of previous measurements, we estimate that the actual resolution for the spectra of Fig. 5(a) was 0.013 Å FWHM, a factor of 2 lower than the nominal resolution. The actual resolution for the spectrum of Fig. 5(b) was expected to be similar to the nominal resolution of 0.05 Å FWHM. The pulsed electric field used for recording the spectrum of Fig. 5(b) was 0.67 V/cm.

The positioning of rotational transitions (N^+, J'') from rotational J'' levels for H_2 to rotational N^+ levels for H_2^+ are marked in Figs. 5(a) and 5(b). By far the strongest peaks in these spectra are the (1,1) transitions. The strength of this transition is shown to result from the coupling with a near-

resonance low-n Rydberg state converging to a high ionization threshold.[28] The resolution of the spectrum shown in Fig. 5(a) is better than that of Fig. 5(b). This is due in part to a better wavelength resolution used in the measurement of the spectrum of Fig. 5(a). In the previous experiment,[18] we had examined the achievable resolution by using a higher wavelength resolution and found that the observed PFI-PE resolution could not be significantly improved because of contamination by strong nearby autoionizing resonances as shown in Fig. 5(b). In view of this previous exercise, we may conclude that the higher resolution observed in Fig 5(a) is due partly to a better suppression of prompt electrons. Nearly all the background peaks originating from strong autoionizing states seen in Fig. 5(b) are suppressed in the spectrum of Fig. 5(a). Two exceptions are the peaks observed at 15.378 and 15.436 eV, which cannot be accounted for by direct ionization processes. These correspond to relatively intense autoionizing states observed in the photoionization cross section[29] and their observation here reflects the fact that suppression of hot electrons is still not complete.

The strongest (1,1) peaks of Figs. 5(a) and 5(b) are normalized to the same intensities. The relative intensities for other rotation transitions observed in Fig. 5(a) are weaker than those resolved in Fig. 5(b). Nevertheless, the relative intensities for (N^+,J'') transitions observed in Figs. 5(a) and 5(b) are in reasonable agreement. Since the spectrum of Fig. 5(a) is essentially free from contamination of autoionizing resonances, it provides a more reliable measure for the relative photoionization cross sections of the marked rotational transitions. Based on the FWHM of the (0,0) transition, we estimate that the PFI-PE resolution for the spectrum of Fig. 5(a) is 2.5 cm^{-1} FWHM, significantly higher than ≈ 7 cm^{-1} FWHM attained in the spectrum of Fig. 5(b). The (0,2) and (4,2) transitions, which completely overlap with the stronger (3,3) and (3,1) transitions, respectively, in Fig. 5(b), are resolved into shoulder peaks in Fig. 5(a). In the present experiment, a doublet is observed at the position of the (2,2) transition. Furthermore, a shoulder peak is evident at the low energy side of the (1,1) transition. The detailed simulation of the H_2^+ PFI-PE spectra using the multichannel quantum defect theory is in progress and will be published elsewhere.[28]

IV. DISCUSSION

The spectra presented in Figs. 4(a), 4(b), 5(a), and 5(b) have demonstrated that the TOF PFI-PE detection method described here is superior compared to the previous synchrotron based PFI-PE measurement schemes[10] in both resolution and background electron suppression. The basic difference between this and the previous arrangement is that the hemispherical energy analyzer is eliminated in the present setup. Consequently, the electron transmission through the analyzer should be higher. Since the TOF axis is perpendicular to the VUV light beam, the TOF resolution is determined only by the height of the VUV beam along the TOF axis. It should be possible to significantly increase the PFI-PE signal by enlarging the entrance and exit apertures of the TOF spectrometer without affecting the TOF resolution. When a 0 V/cm dc electric field is maintained at the PI/PEX region, it is possible to adjusted the height and width of the Stark electric field pulse such that the PFI-PEs formed in the PI/PEX region remain essentially monoenergetic as they travel toward the MSP detector. When this condition is fulfilled, the TOF peak measured by the electron MSP detector is expected to be narrow and be independent of the entrance and exit apertures of the electron TOF spectrometer.

One of the advantage of synchrotron based PFI-PE experiments is that the measured effective lifetimes for high-n Rydberg states are less susceptible to perturbation of ions due to the low ion density produced in a synchrotron experiment.[18,25,26] However, the maximum lifetimes that can be measured by the previous synchrotron based PFI-PE scheme is shown to be limited by the velocity of the neutral Rydberg species and the size of the acceptance aperture for PFI-PE detection.[18,25,26] For example, for an electron acceptance zone defined by a circular aperture of 3 mm in diameter, a thermal Rydberg species of mass 30 amu is expected to move out of the acceptance zone in 2.0 μs. Thus, if the effective lifetime for these high-n Rydberg species is >2.0 μs, it cannot be measured using the previous PFI-PE scheme. Since the TOF PFI-PE detection scheme can be made using large entrance and exit apertures, this limitation for effective lifetime measurements does not apply to this TOF PFI-PE method.

In photoelectron–photoion coincidence (PEPICO) measurements, the extraction of the correlated photoion is often triggered by the arrival of the photoelectron to the electron detector. If the TOF of the photoelectron is long, the correlated ion may move away from the ion detection zone and thus significantly lower the sensitivity of PEPICO measurements. In the present TOF PFI-PE detection scheme, the use of a short TOF spectrometer has shortened the electron TOF from the PI/PEX region to the electron detector to ≈ 50 ns, making it an attractive scheme for coincidence measurements.[30]

ACKNOWLEDGMENTS

This work was supported by the Director, Office of Energy Research, Office of Basic Energy Sciences, Chemical Science Division of the U.S. Department of Energy Under Contract No. W-7405-ENG-82 for the Ames Laboratory and Contract No. DE-AC03-76SF00098 for the Lawrence Berkeley National Laboratory.

[1] *High Resolution Laser Photoionization and Photoelectron Studies*, edited by I. Powis, T. Baer, and C. Y. Ng, Wiley Series in Ion Chemistry and Physics (Wiley, Chichester, 1995).
[2] G. Reiser, W. Habenicht, K. Muller-Dethlefs, and E. W. Schlag, Chem. Phys. Lett. **152**, 119 (1988).
[3] K. Muller-Dethlefs, M. Sander, and E. W. Schlag, Z. Naturforsch. Teil A **39**, 1089 (1984).
[4] D. Valerjo, R. R. Herm, and M. G. Inghram, J. Chem. Phys. **46**, 4495 (1967).
[5] W. B. Peatman, T. B. Borne, and E. W. Schlag, Chem. Phys. Lett. **3**, 492 (1969).
[6] T. Baer, W. B. Peatman, and E. W. Schlag, Chem. Phys. Lett. **4**, 243 (1969).
[7] R. Spohr, P. M. Guyon, W. A. Chupka, and J. Berkowitz, Rev. Sci. Instrum. **42**, 1872 (1971).
[8] E. Waterstradt, R. Jung, H.-J. Deitrich, and K. Muller-Dethlefs, Rev. Sci. Instrum. **64**, 3104 (1993).

[9] R. I. Hall, A. McConkey, K. Ellis, G. Dawber, L. Avaldi, M. A. MacDonald, and G. C. King, Meas. Sci. Technol. **3**, 316 (1992).
[10] C.-W. Hsu, M. Evans, P. A. Heinmann, and C. Y. Ng, Rev. Sci. Instrum. **68**, 1694 (1997).
[11] Y. Morioka, Y. Lu, T. Matsui, T. Tanaka, H. Yoshii, T. Hayaishi, and R. I. Hall, J. Chem. Phys. **104**, 9357 (1996).
[12] K.-M. Weitzel and F. Guthe, Chem. Phys. Lett. **251**, 295 (1996).
[13] W. A. Chupka, J. Chem. Phys. **98**, 4520 (1993).
[14] J. Jortner and M. Bixon, J. Chem. Phys. **99**, 3133 (1995).
[15] T. F. Gallagher, *Rydberg Atoms* (Cambridge University Press, Cambridge, 1994).
[16] C.-W. Hsu, P. A. Heinmann, M. Evans, S. Stimson, T. Fenn, and C. Y. Ng, J. Chem. Phys. **106**, 8931 (997).
[17] C.-W. Hsu, M. Evans, S. Stimson, C. Y. Ng, and P. Heimann, Chem. Phys. **231**, 121 (1998).
[18] S. Stimson, Y.-J. Chen, M. Evans, C.-L. Liao, C. Y. Ng, C.-W. Hsu, and P. Heimann, Chem. Phys. Lett. **289**, 507 (1988).
[19] P. Heinmann, M. Koike, C.-W. Hsu, M. Evans, K. T. Lu, C. Y. Ng, A. Suits, and Y. T. Lee, Rev. Sci. Instrum. **68**, 1945 (1997).
[20] C.-W. Hsu, M. Evans, P. Heinmann, K. T. Lu, and C. Y. Ng, J. Chem. Phys. **105**, 3950 (1996).
[21] A. G. Suits, P. Heinmann, X. Yang, M. Evans, C. W. Hsu, D. A. Blank, K.-T. Lu, A. Kung, and Y. T. Lee, Rev. Sci. Instrum. **66**, 4841 (1995).
[22] R. C. Shiell, M. Evans, S. Stimson, C.-W. Hsu, C. Y. Ng, and J. W. Hepburn, Phys. Rev. Lett. **80**, 472 (1998).
[23] S. Stimson, M. Evans, C. Y. Ng, C. Destandau, G. Chambaud, P. Rosmus, C.-W. Hsu, and P. Heimann, J. Chem. Phys. **108**, 6205 (1998).
[24] C.-W. Hsu, M. Evans, S. Stimson, and C. Y. Ng, J. Chem. Phys. **108**, 4701 (1998).
[25] C.-W. Hsu, M. Evans, S. Stimson, and C. Y. Ng, J. Chem. Phys. **109**, 1285 (1998).
[26] M. Evans, S. Stimson, C. Y. Ng, C.-W. Hsu, and G. K. Jarvis, J. Chem. Phys. **110**, 315 (1999).
[27] H. Palm and F. Merkt, Chem. Phys. Lett. **284**, 419 (1998).
[28] G. K. Jarvis, C.-L. Liao, S. Stimson, M. Evans, Y. Song, S.-Q. Hou, C. Y. Ng, and T. Softley, Phys. Rev. Lett. (to be published).
[29] P. Dehmer and W. A. Chupka, J. Chem. Phys. **65**, 2243 (1976).
[30] G. K. Jarvis, Y. Song, and C. Y. Ng, Rev. Sci. Instrum. (to be published).